ACS OMEGA

Open Access

http://pubs.acs.org/journal/acsodf

Article

Nanocarriers Loaded with Danshensu for Treating Ischemic Stroke by Reducing Oxidative Stress and Glial Overactivation

Cuihong Wang,[‖] Zhicheng Xiao,[‖] Jinhui Fan, Chuan Zhang, Tingfang Wang, Zheng Qiu, Fei Ye,* Min Chen,* and Yi Li*

Cite This: *ACS Omega* 2024, 9, 35686−35694

Read Online

ACCESS | Metrics & More | Article Recommendations | Supporting Information

ABSTRACT: Ischemic stroke is a complex health condition that can cause ischemia and necrosis of brain tissue. Subsequently, the excessive activation of glial cells can result in various inflammatory and oxidative stress reactions that exacerbate ischemic brain injury. In this paper, we propose the targeted self-assembly of a three-dimensional nanoparticle network containing Danshensu to rescue ischemic penumbra by reducing oxidative stress and glial overactivation. The network comprises nanoparticles composed of chitosan, thiol ketone, and carboxymethyl-β-cyclodextrin as the core wrapped by the Pro−His−Ser−Arg−Asn (PHSRN) peptide sequence as the outer layer and loaded with Danshensu. The PHSRN-peptide-modified nanoparticles bind to integrin $\alpha5\beta1$ overexpressed on the damaged blood−brain barrier and accumulate in the damaged brain in a rat model of ischemia/reperfusion. When stimulated by reactive oxygen species, thiol ketone bonded to the nanoparticles was hydrolyzed, facilitating responsive drug release while consuming the reactive oxygen species. Subsequently, the released Danshensu scavenged the reactive oxygen species to prevent oxidative stress and inhibited the activation of astrocytes, thereby suppressing proinflammatory cytokine secretion, improving the inflammatory brain microenvironment and reducing neuronal apoptosis.

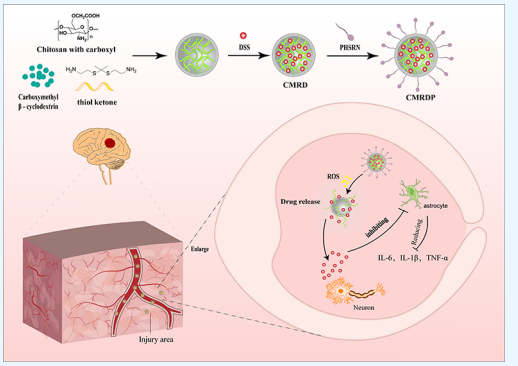

1. INTRODUCTION

Ischemic stroke, which is caused by a sudden blockage due to a thrombus in blood vessels, is the most common type of stroke.[1,2] Restoring blood flow by timely and effective thrombolysis is the gold standard for treating ischemic stroke.[3] However, oxidative stress and inflammation after reperfusion can cause irreparable damage to nerves, negatively affecting the prognosis of ischemic stroke survivors. In addition, the ischemia/reperfusion injury triggered by oxidative stress and inflammation after reperfusion exacerbates the production of reactive oxygen species (ROS) and promotes inflammatory responses that aggravate neuronal damage.[4−7] Notably, key immune cells within the brain, namely, astrocytes and microglia, are prompted to converge around the infarcted area, instigating a cerebral immune response. Particularly, the activation of astrocytes fuels the secretion of inflammatory mediators, such as TNF-α, IL-1β, and IL-17, thereby intensifying the inflammatory cascade. Therefore, the development of more effective strategies for stroke treatment is imperative.

Recently, a nanotechnology-based drug delivery system has been used to improve the delivery efficiency of small-molecule drugs.[8−10] Chitosan (CS), known for its high biocompatibility and nonimmunogenicity, is frequently used as a drug-delivery carrier.[11] However, its limited solubility confines its utility to dilute aqueous acid solutions. Introducing carboxyl groups into the CS structure enhances its water solubility and confers a negatively charged surface, mitigating aggregation and prolonging circulation in the bloodstream.[12,13] Additionally, the distinctive encapsulation properties of β-cyclodextrin make it a valuable medical excipient for improving the hydrophobicity, solubility, stability, and bioavailability of biomolecular drug.[14] Consequently, the combination of chitosan with carboxyl groups and β-cyclodextrin holds promise in the preparation of nanoparticles (NPs) for advanced drug-delivery systems.

Although some nanocarriers can passively deliver drugs to the injury site by increasing permeability and retention, the presence of the blood−brain barrier (BBB) directly mobilizes a considerable proportion of the drug.[15] Receptor-targeted drug delivery offers a solution, exemplified by Pro−His−Ser−Arg−Asn (PHSRN)—a peptide sequence binding specifically to the $\alpha5\beta1$ receptor on damaged brain endothelial cells, facilitating passage through the damaged BBB to directly reach the affected region.[16] Although the advantages of nanotechnology

Received: April 25, 2024
Revised: July 19, 2024
Accepted: July 22, 2024
Published: August 5, 2024

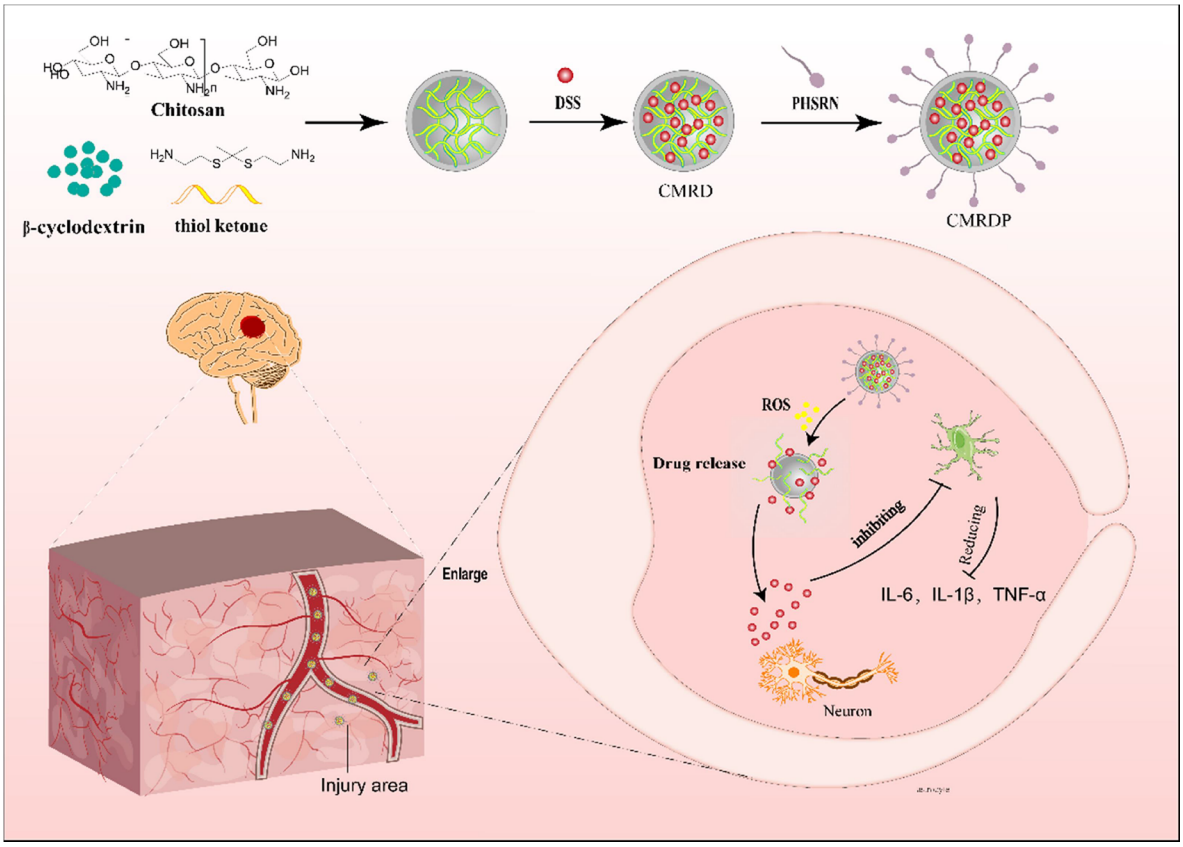

Figure 1. Schematic of the in vivo release of NPs. NPs are intravenously injected into the body and cross the BBB under the action of the PHSRN peptide that enters the brain injury area. Under excessive ROS, the NPs collapse and release DSS, reducing oxidative stress and inhibiting astrocyte overactivation, subsequently reducing the level of production of inflammatory factors and mitigating neuronal apoptosis.

are becoming increasingly apparent, the principles of drugs cannot be ignored. Since 2011, salvianolic acid injection was approved by the Chinese Food and Drug Administration for treating ischemic stroke in clinics.[17] Danshensu (DSS) is one of the main components of salvianolic acid injection; DSS has attracted significant attention owing to its excellent ROS clearance and inflammation-regulation functions.[18,19] However, the strong water solubility and inherent small-molecule properties of DSS considerably hinder it from entering the brain. Therefore, nanodelivery technology must be chosen to effectively target and deliver DSS to the brain. Importantly, our group has previously demonstrated that DSS treatment inhibits oxidative stress, suppresses inflammatory reactions, and decreases neuronal apoptosis in rats, suggesting its potential as a human stroke treatment candidate.[20,21]

In this study, we prepared a three-dimensional (3D) thioketal cross-linked chitosan with carboxyl groups and carboxymethyl β-cyclodextrin network to enhance the efficiency of loading DSS and control its release into injured cerebral regions. This 3D network was first chemically synthesized by linking CS with ketal; subsequently, carboxymethyl β-cyclodextrin were added to form the network. After the addition of DSS, the constituents were linked by intermolecular forces and hydrogen bonds. The target peptide, PHSRN, was then inserted into the gaps in the 3D network, forming the final product, which is a 3D network with ROS responsiveness. In an ischemic-stroke-rat model, intravenously injected NPs entered the brain injury site under the action of targeted peptides. Under the action of ROS, the 3D network dispersed and released DSS, which regulated astrocytes and reduced the production of inflammatory factors, thereby reducing neuronal apoptosis (Figure 1).

2. RESULTS AND DISCUSSION

2.1. Preparation and Characterization of CMRDP NPs.

CMRDP NPs were prepared using a self-assembly method to cross-link CMCOOH and thiol ketone in a solvent of phosphate-buffered saline (PBS) and then coated with carboxymethyl β-cyclodextrin to improve their biocompatibility. After the addition of DSS, it can interact and aggregate with CS, cyclodextrin, or thioketal through H-bonding, become encapsulated in NPs, and finally be modified with target peptide PHSRN on the outer layer to obtain CMRDP NPs (Figure 2A). In our opinion, the successful preparation of CMRDP can be attributed to electrostatic interactions and hydrogen bonding between the molecules. As shown in Figure S1, there is a significant change in the peak of CMRDP between 3200 and 3500 cm^{-1}. At the same time, the free −OH at position B disappears and the position of the unsaturated fatty ketones at position C also changes. These results indicate that several molecules within the nanoparticles associate to form intermolecular H-bonds. Additionally, dynamic light scattering shows that the intensity-average sizes of CMCD, CMRD, and CMRDP NPs are 309.63 ± 1.55, 262.87 ± 6.86, and 202.83 ± 7.56 nm, respectively (Table 1). With the addition of thiol ketone and PHSRN peptides, the size of the nanoparticles gradually decreased. We speculate that this may be due to closer interaction between PHSRN peptides and carboxyl, hydroxyl, or amino groups in the nanoparticles,

https://doi.org/10.1021/acsomega.4c03991
ACS Omega 2024, 9, 35686−35694

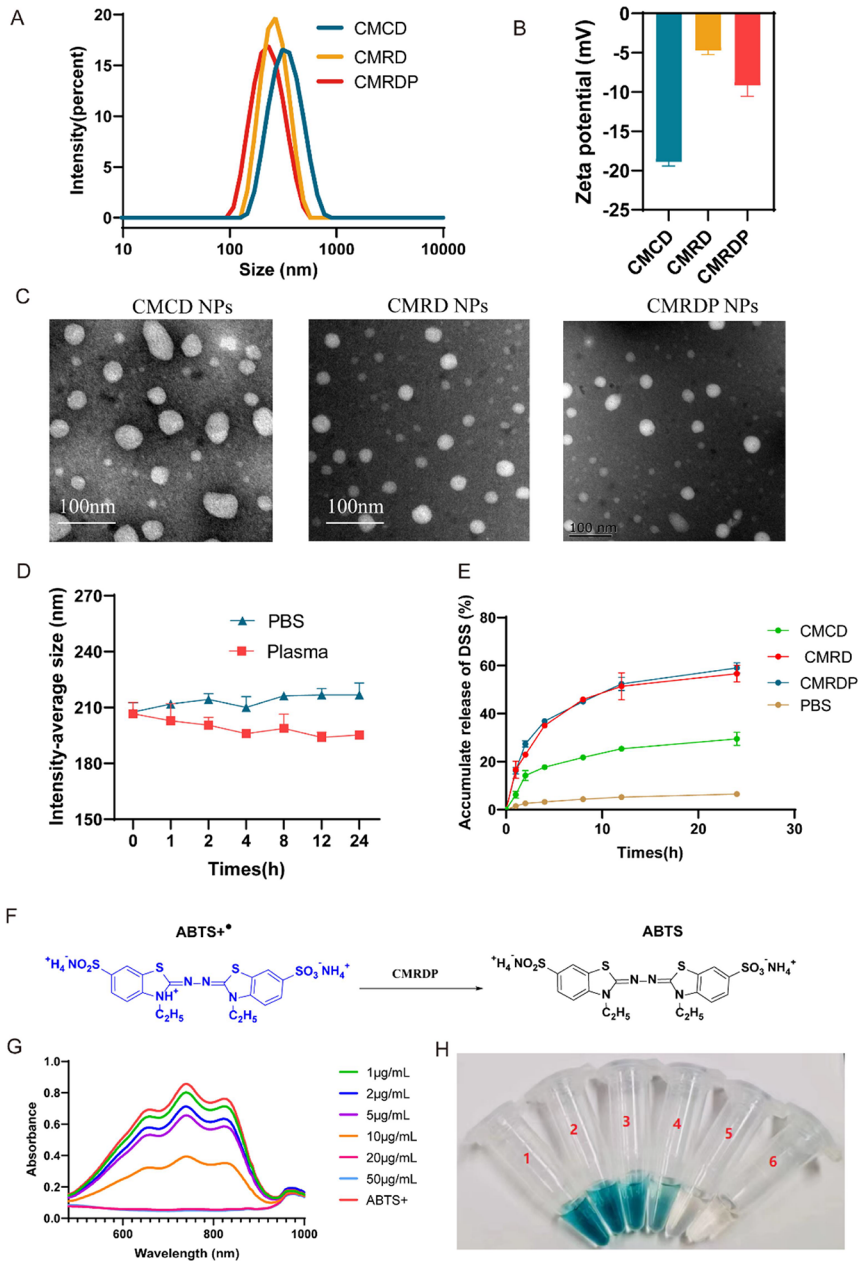

Figure 2. (A) Size and (B) zeta potential detected by dynamic light scattering; n = 3. (C) Typical transmission electron microscopy images of CMRD and CMRDP NPs. (D) Stability of the NPs in PBS and plasma and their size changes; n = 3. (E) DSS release from CMRDP in PBS at 1 mM H_2O_2 and DSS release from CMCD and CMRD in 1 mM H_2O_2. (F) Schematic of the ABTS+● radical scavenging process. (G) UV−vis absorbance spectra. (H) Photograph of ABTS+● radicals after incubation with different concentration gradients of CMRDP NPs. All data are presented as the mean ± SD.

Table 1. Changes in Intensity-Average Size and Zeta Potential of Different Nanoparticles

formation	intensity-average size (nm)	zeta potential (mV)	PDI	EE%	LC%
CMCD	309.63 ± 1.55	−18.91 ± 0.42	0.08 ± 0.02	92.09 ± 0.01	21.92 ± 0.96
CMRD	262.87 ± 6.86	−4.76 ± 0.39	0.29 ± 0.01	92.47 ± 0.01	26.90 ± 0.09
CMRDP	202.83 ± 7.56	−9.19 ± 1.11	0.18 ± 0.01	93.35 ± 0.01	28.17 ± 0.75

increasing nanoparticle stability while decreasing size. The transmission electron microscopy images of the NPs are shown in Figure 2C. After CMCD NPs are added with thioketal linker, the zeta potential increases from ∼ −18.9 ± 0.42 to ∼ −4.76 ± 0.39 mV and decreases to −9.19 ± 1.11 mV when PHSRN is coated, denoting the loading of the thioketal linker and PHSRN into the NPs (Figure 2B). The DSS loading in the CMRDP NPs was measured using high-performance liquid chromatography, capturing the absorption peak at 280 nm, and obtaining a drug-loading rate and entrapment efficiency of 28.17 ± 0.75% and 93.35 ± 0.01%, respectively. In addition, NPs exhibit good stability in different solvents (e.g., PBS and plasma) without obvious changes in the particle size after 24 h

https://doi.org/10.1021/acsomega.4c03991
ACS Omega 2024, 9, 35686−35694

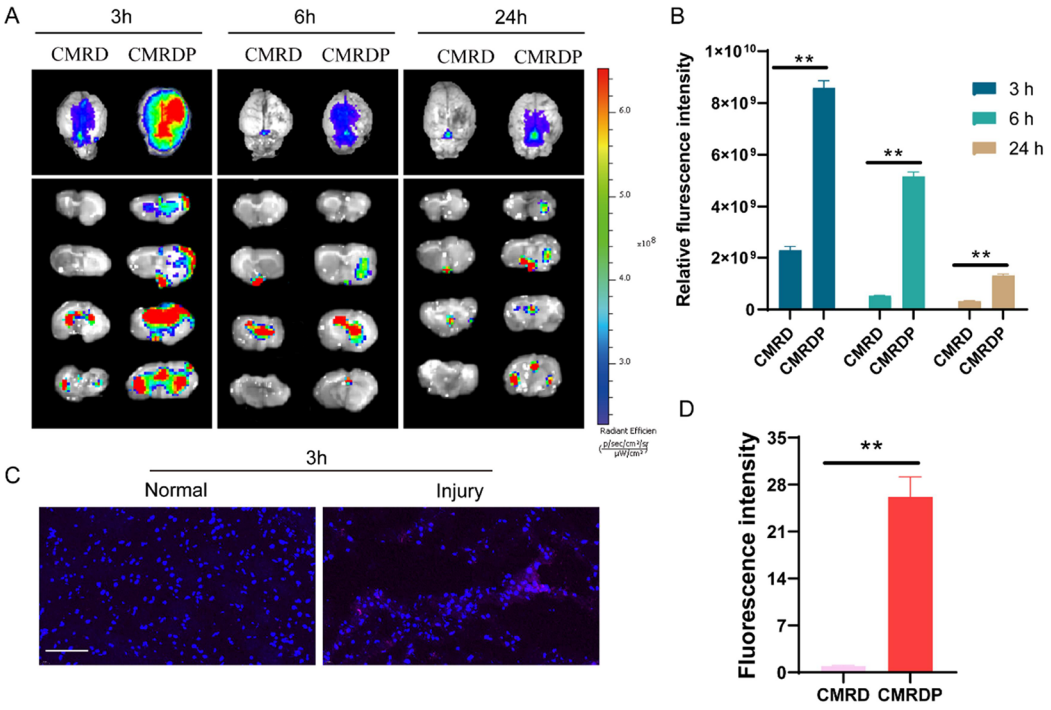

Figure 3. Brain-targeted validation of NP penetration in MCAO/R rats. (A) In vivo fluorescence images of Cy5.5-CMRD and Cy5.5-CMRDP in the entire brain and brain slices from MCAO/R rats at 3, 6, and 24 h post stroke by IVIS Spectrum and (B) fluorescence intensity quantification. (C) Sectioned brain tissue after 3 h of intravenous injection of Cy5.5-CMRD and Cy5.5-CMRDP (scale bar: 100 μm) and (D) fluorescence intensity quantification; n = 3. All data are presented as mean ± SD ** $P < 0.01$.

(Figure 2D), indicating that the NPs can maintain stability in blood.

Hydrogen peroxide, H_2O_2, is one of the main ROS produced during ischemia and reperfusion. The decomposition of H_2O_2 exacerbates cellular oxidative stress.[22] To verify the drug-release profile of CMRDP NPs in vitro, the drug-release profiles of CMRDP NPs in an H_2O_2-simulated in vitro ROS environment and in a normal PBS environment were compared. The DSS release profile demonstrated the rapid release of DSS within 24 h followed by a slow release for 24 h in PBS (Figure 2E), indicating its responsiveness to ROS-releasing drugs for treating ischemic stroke. Furthermore, there was no difference in drug release between CMRD and CMRDP, and the amount released was higher than CMCD, further demonstrating that the addition of ketal made the nanoparticles ROS-responsive.

In addition, we examined the size variations of the NPs across various solvents. The size of the NPs gradually increases in H_2O_2, whereas it remains relatively unchanged in PBS, suggesting that the disintegration of NPs is a continuous process influenced by the ROS concentration[23] (Figure S2). Furthermore, we used the ABTS assay kit, which is commonly used to evaluate antioxidant activity[24] to investigate the total antioxidant capacity of the CMRDP NPs. ABTS+• radicals emit blue-green fluorescence when they are in a high-energy electronic transition state. When antioxidants are added, a chemical reaction reduces them to ABTS molecules, reducing or eliminating the blue-green fluorescence. As the ability of the antioxidant substances to scavenge free radicals increases, the rate at which ABTS+• is reduced to ABTS increases, and the degree of fluorescence decrease increases (Figure 2F). Therefore, the ability of a sample to scavenge free radicals can be qualitatively assessed by measuring the change in absorbance of ABTS before and after the reaction and observing its color change. After the addition of CMRDP to ABTS+•, the color of the solution gradually changes from blue-green to almost colorless with increasing CMRDP concentrations (Figure 2H). Moreover, the characteristic absorption peak of ABTS+• at approximately 738 nm gradually decreases at the same time (Figure 2G), indicating its dose-dependent ROS scavenging ability.[24]

2.2. NPs Crossing BBB and Targeted Accumulation on Site of Middle Cerebral Artery Occlusion/Reperfusion Model In Vivo. The ability of drugs to cross the BBB and precisely target the injury site is the key to treating ischemic stroke.[25] In this study, we established a Sprague–Dawley rat model of middle cerebral artery occlusion/reperfusion (MCAO/R) and investigated the ability of NPs to penetrate the BBB and reach injury sites. Rats were injected with CMRDP NPs through the tail vein, and fluorescence signals of the ischemic brain tissue were observed at different time points using an in vivo imaging system.

Brain tissue fluorescence peaks at 3 h after injection and is concentrated at the site of the right brain injury. The fluorescence decreased after 6 h, and the drug is almost completely cleared after 24 h. Although some CMRD NPs reach the brain at 3 h, they are almost completely metabolized by 6 h, and their retention time in the brain tissue is shorter than that of the CMRDP NPs (Figure 3A,B). This suggests that CMRDP NPs can cross the BBB, aggregate in the area of brain injury, and increase the retention time in brain tissue. Furthermore, we directly sectioned the brain tissue at 3 h after intravenous injection of Cy5.5-labeled CMRDP and observed that several NPs accumulated in the injured brain area. Conversely, the undamaged area is almost invisible, further indicating the accumulation of targeted NPs in the injured

https://doi.org/10.1021/acsomega.4c03991
ACS Omega 2024, 9, 35686−35694

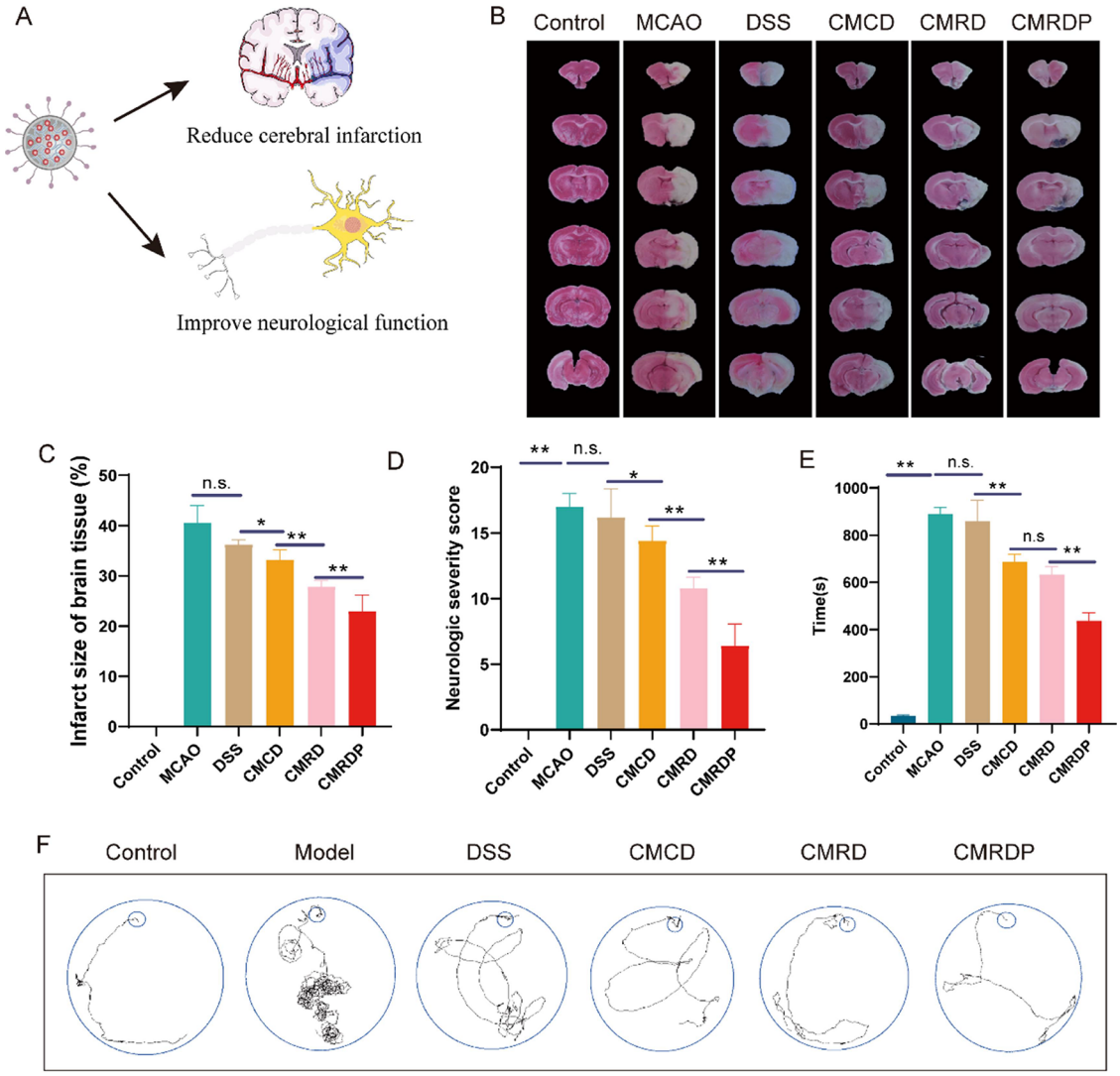

Figure 4. (A) Schematic of the effect of NPs on the brain. (B) Typical TTC staining images of the brain slices in different groups from each treatment group at 7 days post stroke. (C) Quantitative results of cerebral infarct volume from each treatment group (n = 4). (D) Neurological deficits of 2 h MCAO rats from each treatment group (n = 8). (E) Time and (F) trajectory for each group of rats to find the target box in the Barnes maze experiment (n = 4). All data are presented as mean ± SD. n.s. no significance, *p < 0.05, **p < 0.01, ***p < 0.001 (one-way ANOVA with Tukey's post hoc test).

brain area (Figure 3C,D). The blood circulation data reveal that CMRDP initially exhibits a strong fluorescence intensity within the blood. Over time, this fluorescence gradually diminishes, indicating the metabolisation of the NPs (Figure S3). This finding aligns with the results of the IVIS Spectrum.

2.3. CMRDP NPs Alleviating Cerebral Infarction and Improving Neurological Function. To study the therapeutic effects of the CMRDP NPs in vivo, we used an MCAO rat model to test ischemia/reperfusion. After 7 d of continuous administration, 2,3,5-triphenyltetrazolium chloride (TTC) staining was used to detect the presence of cerebral infarction in each group of brain tissues with normal brain tissue stained red and infarcted brain tissue appearing unstained and white (Figure 4A). The infarct volume increases by 40.58 ± 2.97% in the MCAO group and decreases to different degrees after treatment with different drugs, except for the DSS treatment group because of its low dose. The infarct volume of rats in the CMCD treatment group decreases to 33.21 ± 1.77%, and that in the CMRD treatment group significantly decreases to 27.84 ± 1.09%. More encouragingly, the brain infarct volume in the CMRDP treatment group significantly decreases to 22.98 ± 2.74% (Figure 4B,C). Similarly, the CMRDP treatment significantly decreases the neurological severity scores (Figure 4D).

We assessed the neurological recovery in each group of rats by applying the Barnes maze test (Figure 4E,F). The rats from the MCAO group require the longest time to find the target box, and their path is the most intricate. After treatment with different NPs, the time and complexity of the walking trajectory for reaching the target decrease. The CMRDP treatment group exhibits the most considerable decrease, which is significantly lower than that in the CMCD and CMRD treatment groups. However, no difference is observed between the DSS and MCAO groups. Overall, CMRDP has a neuroprotective effect higher than that of CMRD owing to the targeting of PHSRN, which enhances the accumulation of NPs in the brain tissue. CMRD has a better effect than CMCD, which can be attributed to the ROS-linker-targeting system scavenging ROS and improving the therapeutic effect in vivo. The CMRDP treatment group exhibits the best recovery from

https://doi.org/10.1021/acsomega.4c03991
ACS Omega 2024, 9, 35686−35694

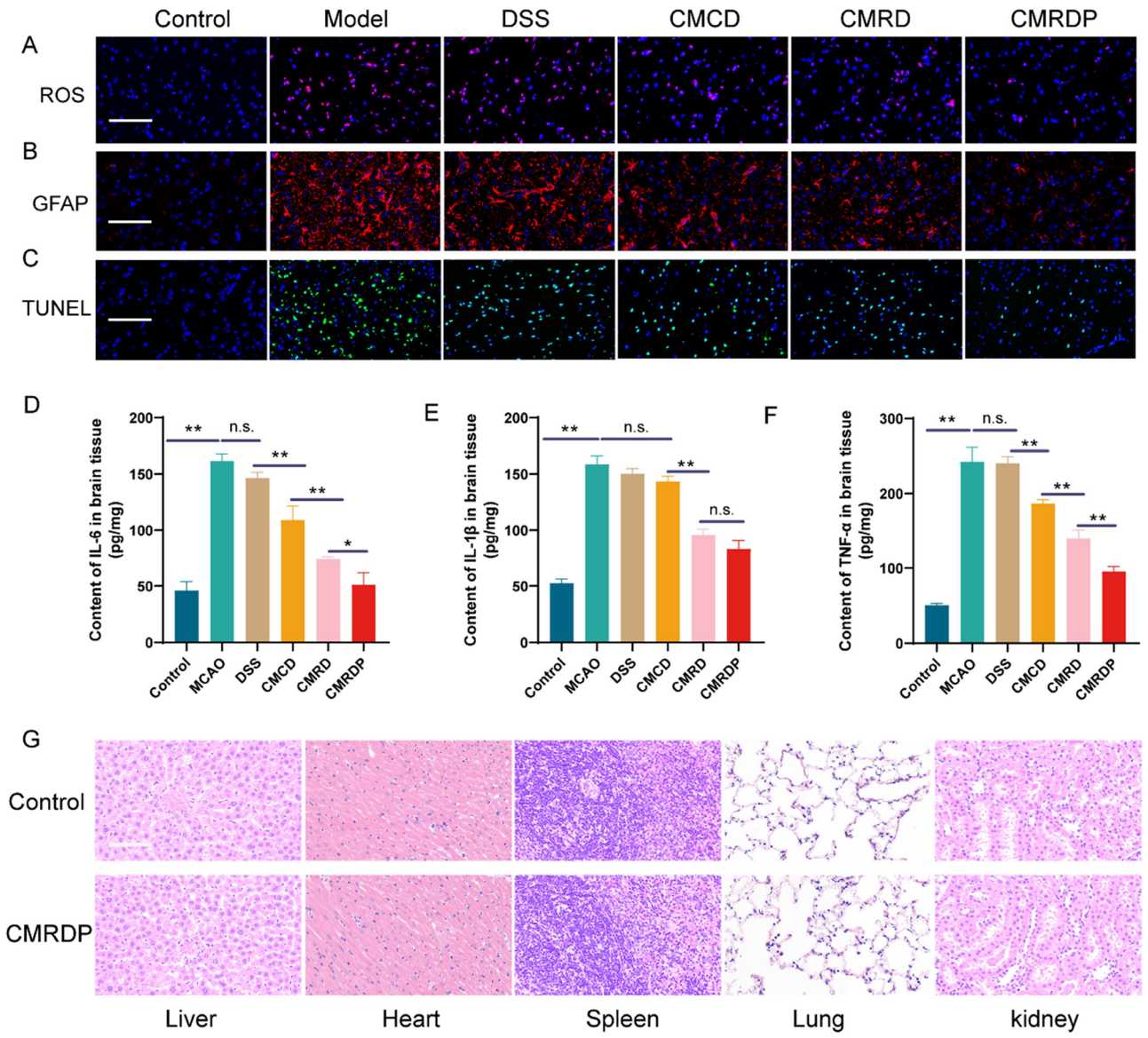

Figure 5. (A) Fluorescence images of brain tissue stained with dihydroethidium probe (scale bar: 100 μm; blue: cell nuclei stained with DAPI; red: ROS). (b) Fluorescence images of brain tissue stained with GFAP (astrocyte marker) antibody (scale bar: 100 μm; blue: cell nuclei stained with DAPI; red: GFAP protein). (c) Typical terminal deoxynucleotidyl transferase dUTP nick end labeling staining images of brain tissue (scale bar: 100 μm). (d) Quantitative results of IL-6, (e) IL-1β, and (f) TNF-α in the ischemic hemisphere from different treatment groups (n = 4). (g) H&E staining of various organs in rats (scale bar: 100 μm). All data are presented as mean ± SD, n.s. no significance, *p < 0.05, **p < 0.01 (one-way ANOVA with Tukey's post hoc test).

cerebral infarction and neurological function, consistent with the TTC staining results.

2.4. CMRDP NPs Improving Ischemic Stroke by Decreasing Oxidative Stress and Glial Overactivation. To further elucidate the mechanism of NP action in an ischemic stroke, we performed an immunohistochemical analysis of brain tissue. Based on the presence of ROS-responsive chains in the NPs, we first measured the ROS levels in brain tissue. The ROS levels in brain tissue of rats in the MCAO group are significantly higher than those in the control group. After CMRDP treatment, the ROS levels significantly decreases in the brain tissue (Figure 5A). Astrocytes are common cells that mediate inflammation following stroke, and glial overactivation may lead to increased expression of inflammatory factors.[26] Therefore, we measured the content of astrocytes by immunofluorescence staining according to the level of inflammatory factors using an enzyme-linked immunosorbent assay for different brain tissues. The immunofluorescence of astrocytes and quantitative results of inflammatory factors indicate a significant increase in the expression of astrocytes and inflammatory factors (i.e., IL-6, IL-1β, and TNF-α). After treatment with CMCD, CMRD, or CMRDP, the expression of inflammatory cytokines decreases in varying degrees with the CMRDP treatment group showing the greatest decrease (Figure 5B,D−F). In addition, the apoptosis of nerve cells decreases to different degrees, consistent with the ROS levels and glial fibrillary acidic protein results (Figure 5C). Overall, CMRDP exerts a robust neuroprotective effect in the brain by eliminating ROS and inhibiting astrocyte overactivation; this subsequently reduces the levels of inflammatory factors and improves the ischemic microenvironment with decreased neuronal apoptosis. Finally,

https://doi.org/10.1021/acsomega.4c03991
ACS Omega 2024, 9, 35686−35694

the safety of the engineered CMRDP was investigated in vivo. Haematoxylin and eosin (H&E) staining indicates the absence of swelling, deformation, or nuclear disintegration in various tissues (Figure 5G), suggesting the good biocompatibility of CMRDP.

3. CONCLUSIONS

NPs loaded with DSS were synthesized by self-assembly and exhibited excellent free-radical-scavenging ability. CMRDP NPs precisely aggregated in the area of brain injury could ameliorate MCAO/R-induced brain injury in rats by reducing oxidative stress and inhibiting astrocytic activation, subsequently reducing neuroinflammation and neuronal apoptosis for optimal improvement of brain infarction. In addition, neurological function and the Barnes maze test indicated that treatment with CMRDP NPs significantly improved deficits in sensory and motor functions and spatial relearning. Overall, our results show that CMRDP NPs have great potential for treating clinical ischemic stroke.

4. MATERIALS AND METHODS

4.1. Materials and Characterization of Nanoparticles. Danshensu (Laboratory self-made), chitosan (Degree of acetylation >80%), and chloroacetic acid was purchased from Adams (Shanghai, China), carboxymethyl β cyclodextrin was purchased from Energy Chemical (Shanghai, China), and PBS was purchased from Adams (Shanghai, China). Sulfur ketal and PHSRN were purchased from Ruixi Biotechnology Co., Ltd. (Shanghai, China). TEM measurements were performed on HT7700 (HITACHI, Japan).

4.2. Animals. SD rat weight 220−250g were purchased from Shanghai Regen Biotechnology Co., Ltd. The procedures for the animal care and all animal experiments were evaluated and approved by the Animal Ethics Committee of Shanghai University School of Medicine (Approval No. ECSHU 2022−182).

4.3. Preparation of Targeting Nanoparticles with ROS-Responsive Chains Loaded with DSS (CMRDP). Briefly, 10 g of chitosan was suspended in propanol, and 30 g of NaOH was added. The mixture was stirred overnight at room temperature. Monochloroacetic acid was then added drop by drop and allowed to react for 4 h at 55 °C. The pH of the solution was adjusted to 7.0, and the CMCS was recovered by washing with 50% ethanol to remove salts, giving carboxylated chitosan (CMCOOH).[27]

PHSRN peptide-modified nanogels (CMRDP) were synthesized as follows: carboxymethyl β-cyclodextrin (4 mL, 1 mg/mL), CMCOOH (8 mL, 2 mg/mL), thiol ketone (1 mL, 5 mg/mL), and DSS (10 mg) were added to reaction for 24 h, and PHSRN (4 mg) was added for another 24 h to afford the CMRDP NPs.[16]

The no targeting nanoparticles with ROS-responsive chains loaded with DSS (CMRD) and no targeting nanoparticles with no ROS responsive chains loaded with DSS (CMCD, prepared by chitosan and β-cyclodextrin loaded DSS) were synthesized like the procedure of CMRDP NPs.

4.4. Drug Encapsulation Efficiency and Loading Capacity. The drug encapsulation efficiency (EE) and loading capacity (LC) of DSS-loaded NPs (CMRDP, CMRD, and CMCD NPs) were investigated as previously described.[36] Briefly, CMRDP, CMRD, and CMCD NPs were dissolved in acetonitrile, vortexed for 1 min, and centrifuged at 10000 rpm for 10 min to remove polymeric materials. The DSS concentration in the supernatant was determined by HPLC (Shimadzu i-Series LC-2050, Japan). The sample injection volume was 20 μL, and the detector wavelength was 280 nm. The encapsulation efficiency (EE) was calculated according to the following formula: EE = $DSS_{encapsulated}/DSS_{total} \times 100\%$, while the drug loading capacity (LC) was calculated according to the formula: LC = $DSS_{encapsulated/materials} \times 100\%$.

4.5. Drug Release Behavior. The in vitro drug release test was carried out in PBS buffer (PH 7.4) and 1 mM H_2O_2. Briefly, a sealed dialysis bag (MWCO = 3500 Da) was filled with 10 mL of CMRDP. The dialysis bag was immersed in PBS buffer (PH 7.4) and 1 mM H_2O_2 solution (40 mL) at 37 °C in the absence of light and shaken at 100 rpm. Liquid samples (200 μL) were taken from the outside of the dialysis bag at specified time points (1, 2, 4, 8, 12, 24 h) and replaced with fresh media (200 μL). DSS was extracted by liquid−liquid extraction and DSS levels were determined by HPLC.

4.6. Stability Testing. The CMRDP NPs was placed in PBS or plasma in a cool and dry environment at room temperature for 24 h, then the samples were taken for testing, and changes in particle size were also recorded.

4.7. Measurement of Free Radical Scavenging Capacity. The radical scavenging capacity of the CMRDP NPs was determined with an ABTS radical scavenging capacity test kit. In brief, the working solutions of ABTS and peroxidase were configured and mixed in advance according to the instructions of the manufacturer. Then, different concentrations (1, 2, 5, 10, 20, and 50 μg/mL) of CMRDP NPs were added to the reaction system. After allowing the mixture to stand at room temperature for 6 min, the absorbance of the mixture was measured at 400−1000 nm using a multifunctional microplate reader (Tecan Spark).

4.8. Establishment and Administration of the MCAO Model. The animals were randomly divided into the following five groups: (a) control group injected with 0.9% NaCl, (b) model group injected with 0.9% NaCl (MCAO), (c) MCAO animal injected with CMRD, (d) MCAO animal injected with CMRDP, (e) MCAO animal injected with CMCD, and (f) MCAO animal injected with DSS. The dosage of nanoparticles is based on the unified standard of DSS 10 mg/kg.

Briefly, the anatomy of the right common, internal, and external carotid arteries was carefully exposed and separated from the surrounding tissue after ventral midline cervical dissection. Once the lateral branch was ligated, a custom-made silicone-coated Nylon monofilament thread was inserted from the external carotid, blocking the origin of the middle left cerebral artery. After 2 h of occlusion, reperfusion was induced by the gentle withdrawal of the monofilament thread. Sham rat groups underwent a procedure identical to that of MCAO except that the monofilament was not inserted.

4.9. Longa Scoring and Barnes Maze. Neurological deficits were assessed 24 h prior to sacrifice by using the Longa scale, as described previously. In detail, 0, no apparent neurological deficits; 1: cannot extend the affected forelimb; 2: walking in circles; 3: not evenly balanced while walking; and 4: numb and cannot walk. The observation was blinded to the group assignment. The rats scoring 1−3 points after MCAO/R were indicated for successful modeling and were eligible for the following study.

To monitor the improvement in cognitive and memory performance in treated rats, the rats were placed in the Barnes maze, first acclimating to the target box for 30 s, and then

https://doi.org/10.1021/acsomega.4c03991
ACS Omega 2024, 9, 35686−35694

placed on the opposite side of the target box. The whole procedure was performed in the dark. Following stimulation with strong light, the rats entered the target box, and the time and distance covered in the maze within 10 min were recorded. Rats that did not enter the target box within 10 min were excluded.

4.10. Targeting of CMRDP NPs In Vivo. In order to monitor the accumulation of CMRDP NPs in the brain after MCAO in vivo, male SD rats were subjected to a single intravenous administration of cy5.5-labeled CMRD and CMRDP NPs (20 mg/kg). Biofluorescent imaging was performed 3, 6, and 24 h after injection (VISQUE Invivo Elite, Vieworks, Korea).

4.11. TTC and H&E Staining. Triphenyltetrazolium chloride (TTC) staining was used to observe the infarct volume. Briefly, the brain was cut into 6 slices (2 mm-thick) and stained with 2% TTC PBS solution. Brain slices were rotated every 2 min to ensure even staining, then fixed in 4% paraformaldehyde, and photographed using a digital camera. Infarct volume was measured using the ImageJ analysis system. The cerebral infarct volume was calculated using the following formula: infarct volume (%) = (contralateral hemisphere volume − noninfarcted ipsilateral hemisphere volume)/contralateral hemisphere volume × 100%. To assess brain infarction by immunohistochemistry, brain tissues were cut into 4 μm-thick sections for hematoxylin-eosin (H&E).

4.12. Immunohistochemistry and Immunofluorescence. At the end of the assay, we euthanized the mice, perfused the hearts with PBS and 4% paraformaldehyde, and sliced the brains into 10 μm coronal slices. The slices were fixed, sealed, and incubated with primary antibodies at 4 °C overnight. The following primary antibodies were used GFAP antibody (XY-KF720, rabbit, 1:100, CST). The following second antibodies were used: goat antirabbit Alexa Fluor 488 conjugate (1:200), goat antirabbit (1:10000). Additionally, Tunel staining was performed using TUNEL kit, ROS labeled with DHE, and nucleus stained with DAPI. Imaging was performed with a Nikon A1Si confocal microscope (Nikon, Japan). ImageJ 1.41 software was used to analyze colocalization images and positive area percentage images.

4.13. Enzyme-Linked Immunosorbent Assay (ELISA). ELISA was used to detect the levels of expression of inflammatory factors, TNF-α, IL-1β, and IL-6 in ischemic stroke brain tissues. After treatment, ischemic brains were collected and lysed with a RIPA lysis buffer (Solarbio, China). Tissue lysates were centrifuged at 14 000 rpm for 5 min, and supernatants were collected for measuring the total protein concentration. Experiments were conducted according to the ELISA kit protocol.

4.14. Statistical Analysis. All of the experiments were carried out in triplicate. One-way analysis of variance (ANOVA) test was used for statistical difference analysis.

■ ASSOCIATED CONTENT

Supporting Information

The Supporting Information is available free of charge at https://pubs.acs.org/doi/10.1021/acsomega.4c03991.

> Infrared spectroscopy detected the changes in chemical bonds of various compounds and nanoparticles, the changes in nanoparticle size across different solvents, and IVIS spectroscopy monitored the in vivo blood circulation of CMRDP NPs (PDF)

■ AUTHOR INFORMATION

Corresponding Authors

Fei Ye − *411 Hospital of Shanghai University, School of Medicine, Shanghai University, Shanghai 200444, China*; Email: yefei_5682@163.com

Min Chen − *Department of Pharmacy, Shanghai University of Medicine and Health Sciences Affiliated Zhoupu Hospital, Shanghai 201318, China*; Email: 13817058298@163.com

Yi Li − *411 Hospital of Shanghai University, School of Medicine, Shanghai University, Shanghai 200444, China*; orcid.org/0000-0003-1138-7311; Email: liyi4868@shu.edu.cn

Authors

Cuihong Wang − *Department of Pharmacy, Shanghai University of Medicine and Health Sciences Affiliated Zhoupu Hospital, Shanghai 201318, China*

Zhicheng Xiao − *411 Hospital of Shanghai University, School of Medicine, Shanghai University, Shanghai 200444, China*

Jinhui Fan − *411 Hospital of Shanghai University, School of Medicine, Shanghai University, Shanghai 200444, China*

Chuan Zhang − *411 Hospital of Shanghai University, School of Medicine, Shanghai University, Shanghai 200444, China*

Tingfang Wang − *411 Hospital of Shanghai University, School of Medicine, Shanghai University, Shanghai 200444, China*; orcid.org/0000-0002-0927-9023

Zheng Qiu − *Shenzhen Medicines and Health Products IMP. & EXP. Co., Ltd., Guangdong 518000, China*

Complete contact information is available at: https://pubs.acs.org/10.1021/acsomega.4c03991

Author Contributions

‖C.W. and Z.X. contributed equally as the first author.

Notes

The authors declare no competing financial interest.

■ ACKNOWLEDGMENTS

This work was supported by the Science and Technology Support Project in Biomedical Field of the Science and Technology Innovation Action Plan of Shanghai Science and Technology Commission (Grant No. 21S21902100), Baoshan Zhaohui New Drug R&D, Transformation Functional Platform (Grant No. 2021-HSD-8-6-001), and Shanghai Pudong New Area Health System Excellent Young Medical Talents Training Program (PWRq2022-40).

■ REFERENCES

(1) GBD 2019 Ethiopia Subnational-Level Disease Burden Initiative Collaborators. Progress in health among regions of Ethiopia, 1990−2019: a subnational country analysis for the Global Burden of Disease Study 2019. *Lancet* **2022**, *399* (10332), 1322−1335.

(2) Martin, S. S.; Aday, A. W.; Almarzooq, Z. I.; et al. 2024 Heart Disease and Stroke Statistics: A Report of US and Global Data From the American Heart Association. *Circulation* **2024**, *149* (8), e347−e913.

(3) CAO, H.; SETO, S. W.; BHUYAN, D. J.; et al. Effects of Thrombin on the Neurovascular Unit in Cerebral Ischemia. *Cellular and molecular neurobiology* **2022**, *42* (4), 973−84.

(4) LI, C.; SUN, T.; JIANG, C. Recent advances in nanomedicines for the treatment of ischemic stroke. *Acta pharmaceutica Sinica B* **2021**, *11* (7), 1767−88.

(5) LV, W.; XU, J.; WANG, X.; et al. Bioengineered Boronic Ester Modified Dextran Polymer Nanoparticles as Reactive Oxygen Species

Responsive Nanocarrier for Ischemic Stroke Treatment. *ACS Nano* **2018**, *12* (6), 5417−26.
(6) NOZOHOURI, S.; SIFAT, A. E.; VAIDYA, B.; et al. Novel approaches for the delivery of therapeutics in ischemic stroke. *Drug discovery today* **2020**, *25* (3), 535−51.
(7) YOU, Y.; XU, J.; LIU, Y.; et al. Tailored Apoptotic Vesicle Delivery Platform for Inflammatory Regulation and Tissue Repair to Ameliorate Ischemic Stroke. *ACS Nano* **2023**, *17* (9), 8646−62.
(8) FENG, L.; DOU, C.; XIA, Y.; et al. Neutrophil-like Cell-Membrane-Coated Nanozyme Therapy for Ischemic Brain Damage and Long-Term Neurological Functional Recovery. *ACS Nano* **2021**, *15* (2), 2263−80.
(9) LIAO, J.; FAN, L.; LI, Y.; et al. Recent advances in biomimetic nanodelivery systems: New brain-targeting strategies. *Journal of controlled release: official journal of the Controlled Release Society* **2023**, *358*, 439−64.
(10) LIAO, J.; LI, Y.; LUO, Y.; et al. Recent Advances in Targeted Nanotherapies for Ischemic Stroke. *Mol. Pharmaceutics* **2022**, *19* (9), 3026−41.
(11) YANG, C.; WANG, X.; YAO, X.; et al. Hyaluronic acid nanogels with enzyme-sensitive cross-linking group for drug delivery. *Journal of controlled release: official journal of the Controlled Release Society* **2015**, *205*, 206−17.
(12) PANDYA, A. D.; ØVERBYE, A.; SAHARIAH, P.; et al. Drug-Loaded Photosensitizer-Chitosan Nanoparticles for Combinatorial Chemo- and Photodynamic-Therapy of Cancer. *Biomacromolecules* **2020**, *21* (4), 1489−98.
(13) WANG, H.; ZHANG, Y.; XUE, W.; et al. Preparation, characterization and antibacterial activity of a novel soluble polymer derived from xanthone and O-carboxymethyl-N, N, N-trimethyl chitosan. *Int. J. Biol. Macromol.* **2020**, *164*, 836−44.
(14) NONSUWAN, P.; PHIBOONCHAIYANAN, P. P.; HIRUN, N.; et al. Curcumin-loaded methacrylate pullulan with grafted carboxymethyl-β-cyclodextrin to form hydrogels for wound healing: In vitro evaluation. *Carbohydr. Polym.* **2023**, *321*, No. 121294.
(15) LUIZ, M. T.; DELELLO DI FILIPPO, L.; TOFANI, L. B.; et al. Highlights in targeted nanoparticles as a delivery strategy for glioma treatment. *International journal of pharmaceutics* **2021**, *604*, No. 120758.
(16) Yang, H.; Lou, Y.; Hu, H.; et al. pH-Sensitive, Cerebral Vasculature-Targeting Hydroxyethyl Starch Functionalized Nanoparticles for Improved Angiogenesis and Neurological Function Recovery in Ischemic Stroke. *Adv. Healthcare Mater.* **2021**, *10* (12), No. e2100028.
(17) LING, Y.; JIN, L.; MA, Q.; et al. Salvianolic acid A alleviated inflammatory response mediated by microglia through inhibiting the activation of TLR2/4 in acute cerebral ischemia-reperfusion. *Phytomedicine* **2021**, *87*, No. 153569.
(18) LI, Y.; LUO, Y.; WANG, J.; et al. Discovery of novel danshensu derivatives bearing pyrazolone moiety as potential anti-ischemic stroke agents with antioxidant activity. *Bioorganic chemistry* **2023**, *131*, No. 106283.
(19) ZHANG, S.; KONG, D. W.; MA, G. D.; et al. Long-term administration of salvianolic acid A promotes endogenous neurogenesis in ischemic stroke rats through activating Wnt3a/GSK3β/β-catenin signaling pathway. *Acta pharmacologica Sinica* **2022**, *43* (9), 2212−25.
(20) Li, Y.; Liao, J.; Xiong, L.; et al. Stepwise targeted strategies for improving neurological function by inhibiting oxidative stress levels and inflammation following ischemic stroke. *J. Controlled Release* **2024**, *368*, 607.
(21) Yang, S.; Chen, H.; Su, W.; et al. Protective effects of Salvianic acid A against multiple-organ ischemia-reperfusion injury: a review. *Front. Pharmacol.* **2023**, *14*, No. 1297124.
(22) DOU, Y.; LI, C.; LI, L.; et al. Bioresponsive drug delivery systems for the treatment of inflammatory diseases. *Journal of controlled release: official journal of the Controlled Release Society* **2020**, *327*, 641−66.
(23) LI, J.; ANRAKU, Y.; KATAOKA, K. Self-Boosting Catalytic Nanoreactors Integrated with Triggerable Crosslinking Membrane Networks for Initiation of Immunogenic Cell Death by Pyroptosis. *Angewandte Chemie (International ed in English)* **2020**, *59* (32), 13526−30.
(24) LI, X.; HAN, Z.; WANG, T.; et al. Cerium oxide nanoparticles with antioxidative neurorestoration for ischemic stroke. *Biomaterials* **2022**, *291*, No. 121904.
(25) PARVEZ, S.; KAUSHIK, M.; ALI, M.; et al. Dodging blood brain barrier with ″nano″ warriors: Novel strategy against ischemic stroke. *Theranostics* **2022**, *12* (2), 689−719.
(26) Liu, M.; Xu, Z.; Wang, L.; et al. Cottonseed oil alleviates ischemic stroke injury by inhibiting the inflammatory activation of microglia and astrocyte. *J. Neuroinflammation* **2020**, *17* (1), 270.
(27) SONG, P.; SONG, N.; LI, L.; et al. Angiopep-2-Modified Carboxymethyl Chitosan-Based pH/Reduction Dual-Stimuli-Responsive Nanogels for Enhanced Targeting Glioblastoma. *Biomacromolecules* **2021**, *22* (7), 2921−34.

https://doi.org/10.1021/acsomega.4c03991
ACS Omega 2024, 9, 35686−35694